



Parametric analysis of solid oxide fuel cell fueled by syngas based on lattice Boltzmann method

Yongqi Wei¹ · Zhi Ning¹ · Chunhua Sun² · Ming Lv¹ · Yechang Liu¹

Received: 23 November 2023 / Revised: 24 January 2024 / Accepted: 20 February 2024 / Published online: 27 February 2024
© The Author(s), under exclusive licence to Springer-Verlag GmbH Germany, part of Springer Nature 2024

Abstract

During the operation progress of solid oxide fuel cell (SOFC), the performance and endurance are two major concerns significantly affected by gas flowing, charge transport, and chemical reaction. This paper presents a thorough research on the key parameters related to syngas and charge transport in the SOFC to reveal the intrinsic influence mechanism, including electro conductivity, gas mixture concentration, CH₄ component ratio, temperature, and anode thickness, which is instrumental in improving the operational efficiency and applicability of SOFC. Firstly, the theoretical models of charge transport and multi-component mass transfer are established, respectively, and the two are coupled using the reaction rate calculation method. Then, employing an innovative combination of the representative elementary volume (REV) scale lattice Boltzmann method (LBM) and the finite-difference LBM, the potential and multi-component gases distributions are simulated to calculate the evaluated indicators, namely activation and concentration overpotential. Finally, considering various operational conditions, the simulation experiments are conducted to investigate the parametric effect on the performance of SOFC fueled by syngas. The results demonstrate that compared to the direct reforming way, the external syngas with lower CH₄ component ratio is more favorable to the SOFC and the optimal ratio should be controlled within 0.2. The higher concentration of gas mixture and lower anode thickness both contribute to weakening the effect of concentration polarization. Especially, the performance of SOFC is improved when the concentration is 15 mol·m⁻³ and the anode thickness is below 1.05 mm. With the increment of conductivity and operating temperature, the consumption of H₂ gradually increases, enhancing the efficiency of reaction gas and reducing the economic cost. And the optimal operation temperature of SOFC is about 1073 K. Moreover, the anode thickness is a trade-off between the electrochemical reaction conditions of anode and cathode, as its variation affects both of them.

Keywords Solid oxide fuel cell · Mass transfer · Charge transport · External syngas · Lattice Boltzmann method · Concentration polarization

Introduction

Underwater unmanned vehicle (UUV) with long endurance plays a core role in the deep-sea exploration. To meet its the power requirements, the solid oxide fuel cell (SOFC) with advantages of high electric efficiency and stable performance stands out as a promising energy device. One characteristic of the SOFC is simple structure, mainly consisting

of the anode channels, porous anode, cathode channels, porous cathode and electrolyte [1]. According to the different thickness of porous anode and cathode, the SOFC can be classified into two types: anode-supported SOFC and cathode-supported SOFC. Especially, the former has gained increasing attention due to its superior operational performance [2]. The other characteristic is high fuel flexibility. Apart from the hydrogen (H₂), the anode can also be supplied with a gas mixture of methane (CH₄) and steam (H₂O), as well as syngas.

When fuel gases are fueled to the cathode and anode, they flow into the triple phase boundary (TPB), that is, the interface among gas species, charge conductor and catalyzer. At the TPB, an electrochemical reaction takes place to produce the electrons (e⁻), which are collected to meet the energy

✉ Chunhua Sun
11116347@bjtu.edu.cn

¹ School of Mechanical, Electronic and Control Engineering, Beijing Jiaotong University, Beijing 100044, China

² Shanghai Marine Diesel Engine Research Institute, Shanghai, China

demand of external loads. In the electrolyte, only oxygen ions (O^{2-}) flow, while in the porous anode and cathode, both mass transfer and charge transport occur, resulting in a multi-physics field coupling and thus affecting the performance of SOFC.

The performance of SOFC can be improved by supplying a gas mixture of CH_4 and H_2O or syngas in comparison to the H_2 only. However, the possibility of carbon deposition may increase owing to the gas mixture of CH_4 and H_2O , which leads to the structural damage of SOFC [3]. Therefore, the syngas obtains extending application. To enhance the performance and efficiency of SOFC, it is crucial to investigate the coupled physical and chemical processes in the porous anode and cathode fueled by syngas, which is also beneficial to promote the application of SOFC in the engineering.

Nonetheless, it is very difficult to directly monitor the charge transport and mass transfer in the porous cathode and anode [4, 5]. In order to study the characteristic of multi-physics field coupling in the porous cathode and anode, the computational fluid dynamic (CFD) based on the simulation model of SOFC proves to be an effective tool, including physical model and numerical method.

The physical models are generally employed to simulate the charge transport and mass transfer, such as dusty gas model (DGM), Stefan Maxwell model (SMM), Brinkman model and Fick's model (FM) [6]. And the models, solved by adopting the traditional numerical methods like the finite difference method (FDM), the finite volume method (FVM) and the finite element method (FEM) are called the macroscopic model. Kasra Nikooyeh et al. developed a three-dimensional (3D) macroscale model to explore the thermal and electrochemical behavior of SOFC by directly reforming the CH_4 internally. The results concluded that the gas mixture of CH_4 and H_2O can dilute the fuel concentration and the performance of SOFC is decreased. Even worse, there is a carbon deposition in the porous anode [7]. Through the combination of the DGM and the FVM, Meng Ni researched the transport and reaction processes of SOFC fueled by syngas. They found that compared to the H_2 -fueled SOFC, the performance of SOFC is slightly decreased with an increase of gas velocity [8], but the component ratio of CH_4 remained higher.

Since the mass transfer mainly involves Knudsen and molecular diffusion, which belong to the mesoscale mechanisms, the simulation results based on the macro-scale models exhibit comparatively low accuracy and are unsuitable for the in-depth study of mass transfer. Thus, adopting the lattice Boltzmann method (LBM) to solve the physical model attracts more and more prominence, which could improve the simulation accuracy of mesoscale models.

To validate the feasibility of LBM-based model for simulating the SOFC, Grew conducted a study of

electrochemical and gas transfer in the anode using the LBM, which contributed to enhancing the accuracy of simulation results [9]. Aiming at the representative elementary volume (REV) of SOFC and concentration polarization, Xu et al. designed a 2D multi-component LBM-based model to simulate mass transfer in both the porous cathode and anode [10]. Furthermore, the LBM can be combined with other numerical methods to simulate the process of multi-component gas transport. Dang designed a binary gas mixture finite-difference LBM to study the H_2 transport, which has been proved to simulate the flow with larger ratio of molecular weights [11]. Xu built a pore scale LB model to predict the gas species distributions in the anode, fed with the gas mixture of CH_4 and H_2O [45]. However, the direct internal reforming in the anode would cause carbon deposition, which is detrimental to the performance of SOFC.

The LBM-based models can also be used to simulate other physical fields. For example, Xu established a numerical LBM-based model to predict the potential distribution of the pattern anode and calculate the reaction current density at TPB [12], but the coupling between mass transfer and charge transport was not considered.

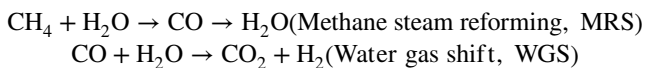
As previously mentioned, the mixture of CH_4 and H_2O is harmful to the performance of SOFC [20]. A more favorable approach is to externally reform CH_4 to produce the syngas, including CH_4 , H_2 , H_2O , CO and CO_2 , and then supply the gas mixture to the anode, namely the external syngas, which can help to prevent the carbon deposition and maintain the performance of SOFC. Although the mesoscale models are widely employed to simulate the charge transport and multi-component mass transfer in SOFC, there still exist some deficiencies. One of deficiencies is that there are limited researches on the external syngas flowing in the porous anode. The other is that the mesoscale model is usually used to model the charge transport or mass transfer in the porous electrode, while few researches focus on the multi-physics field coupling.

Aiming at the SOFC fueled by external syngas, this paper conducts a thorough research on the effect of key parameters on potential distributions and concentration polarization of SOFC, which can provide a theoretical support for the operation strategy and structure optimization of SOFC. Firstly, the physical models of charge transport and multi-component mass transfer are established and coupled by means of the reaction rate calculation method. Secondly, innovatively combining the REV scale LBM with finite-difference LBM, the potential and gas species distributions in the porous cathode and anode are predicted. Based on this, three indicators, namely activation polarization, concentration polarization and ohmic polarization, are calculated to quantitatively evaluate the operational performance of SOFC. Finally, taking different

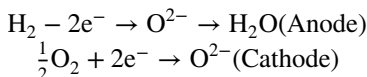
operational cases into account, the operation mechanism and performance of SOFC fueled by syngas are investigated comprehensively.

Mathematical models

At present, the numerical model is based on the following assumptions: isothermal, steady state, isotropic, and laminar flow in the gas mixture. By adding the reformer in the SOFC system, the syngas is supplied into anode. In the external syngas, there are five components, that is, CH₄, H₂, carbon monoxide (CO), H₂O and carbon dioxide (CO₂). The methane reforming reaction (MRS) occurs between H₂O and CH₄ [13, 14], and the water gas shift reaction (WGS) also occurs between H₂O and CO [15–19], expressed as follows.



According to the electrochemical reaction between H₂ and oxygen (O₂) [20, 43, 44], H₂ is consumed to produce the H₂O due to the O²⁻ flowing, which can be written as follows.



The charge transport and multi-component gas transfer are shown in Fig. 1. The gas concentration at the TPB is lower than at the inlet, which results in a decrease in potential. The drop potential is known as the concentration overpotential. Compared to lower current densities, the impact of higher current densities on the concentration polarization is more significant. Another two types

of polarization are activation overpotential and ohmic overpotential.

Charge transport model

It is appropriate to describe the process of charge transport by using the Poisson equation, which is as follows [1],

$$\nabla^2 \varphi = 0 \tag{1}$$

where φ is the electrostatic potential.

Multi-component mass transfer model

In order to describe the mass transfer in the cathode and anode, the Brinkman model is employed. The continuity, momentum and species equation are as follows [10],

$$\nabla \cdot \vec{u} = 0 \tag{2}$$

$$\nabla p = -\frac{\nu}{K} \vec{u} + \nu_{eff} \nabla^2 u \tag{3}$$

$$\nabla \cdot \vec{I}_A = \dot{S}A \tag{4}$$

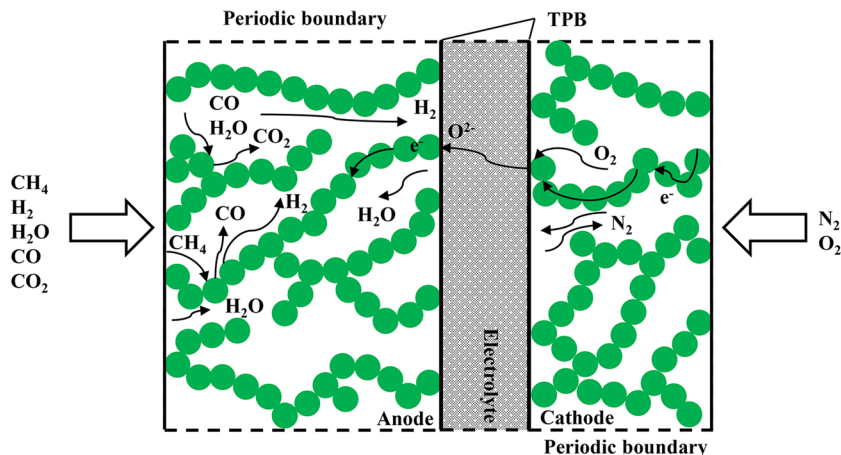
where \vec{u} is the velocity of gas mixture, p is the pressure, K is the permeability, ν is the viscosity of gas, ν_{eff} is the effective viscosity, I_A is the mass flux of gas species A, \dot{S} is the source term.

Reaction rate calculation method

The current density at TPB is written as Eq. (5) [21],

$$i_{TPB} = i_{ex} \left\{ \exp\left(\frac{anF}{RT} \eta_{act}\right) - \exp\left(\frac{-anF}{RT} \eta_{act}\right) \right\} \tag{5}$$

Fig. 1 Schematic of charger transfer and multi-component diffusion through representative domain of SOFC



where i_{TPB} is the current density at TPB, i_{ex} is the exchange current density, α is the transfer coefficient, n is the electronic exchange coefficient, R is the universal gas constant, T is the operation temperature, F is the Faraday constant.

Because of electrochemical reaction, the consumption of H_2 is calculated based on the Faraday’s law, as follows [12],

$$j_{H_2} = \frac{i_{TPB}}{nF} \tag{6}$$

where j is the molar flux of H_2 ,

The reaction rates of MSR and WGS are calculated by Eqs. (7)–(8) [15],

$$r_r = p^2 [k_{fr} \gamma_{CH_4} \gamma_{H_2O} - p^2 k_{br} \gamma_{H_2}^3 \gamma_{CO}] \tag{7}$$

$$r_s = p^2 [k_{fs} \gamma_{CO} \gamma_{H_2O} - k_{bs} \gamma_{CO_2} \gamma_{H_2}] \tag{8}$$

where

$$k_{fr} = 2395 \times \exp\left(-\frac{231266}{RT}\right) \tag{9}$$

$$k_{fs} = 0.0171 \times \exp\left(-\frac{103191}{RT}\right) \tag{10}$$

The reaction rates of five components at TPB are formulated as follows [20].

$$\begin{cases} \dot{S}_{CH_4} = -r_r \times M_{CH_4} \\ \dot{S}_{H_2} = (3r_r + r_s - j_{H_2}) \times M_{H_2} \\ \dot{S}_{H_2O} = (-r_r - r_s + 2j_{H_2}) \times M_{H_2O} \\ \dot{S}_{CO} = (r_r - r_s) \times M_{CO} \\ \dot{S}_{CO_2} = r_s \times M_{CO_2} \end{cases} \tag{11}$$

Lattice Boltzmann method

The charge and multi-component conversation equations are solved by the REV scale LBM and the finite-difference LBM, respectively. In the finite-difference LBM, the continuity gas is regarded as a lot of gas molecules, and the gas flow is regarded as the irregular motion of gas molecules [22, 23].

LBM for charge transport

The individual movements of large number electrons and ions are paid more attention in the LBM. There are two steps to using the LBM, which are the collision and streaming. In this research, the D_2Q_9 (2-dimensional 9-velocity) model is adopted [24, 25].

During the process of collision, Eq. (1) is solved by the following equation [26],

$$f_y(\vec{x} + \vec{e}_y \delta_t, t + \delta_t) - f_y(\vec{x}, t) = -\frac{1}{\tau_c} (f_y(\vec{x}, t) - f_y^{eq}(\vec{x}, t)) \tag{12}$$

where f_y is the distribution function with velocity \vec{e}_y at the lattice site \vec{x}_y and time t , τ_c is the collision time. The equilibrium distribution function f_y^{eq} is calculated as,

$$f_y^{eq}(\vec{x}, t) = \omega_y \varphi(\vec{x}, t) \tag{13}$$

where y is the streaming direction of electrons and ions, ω_y is the weight function of every direction. For the D_2Q_9 model, the streaming direction is shown in Fig. 2.

In different directions, the streaming numbers of electrons and ions are different. The weight function ω_y is given in the following equations [4],

$$\omega_y = \begin{cases} \frac{4}{9}, y = 0 \\ \frac{1}{9}, y = 1, 2, 3, 4 \\ \frac{1}{36}, y = 5, 6, 7, 8 \end{cases} \tag{14}$$

According to the specific direction, the distribution function at the different nodes can be obtained with the help of electrons and ions streaming processes. In order to recover Eq. (1), the moment of distribution functions is employed via Chapman-Enskog expansion, which is as follows,

$$\varphi(\vec{x}, t) = \sum_y f_y(\vec{x}, t) \tag{15}$$

At the interface between the porous electrodes and electrolyte, the voltage difference is the activation polarization which is obtained [1],

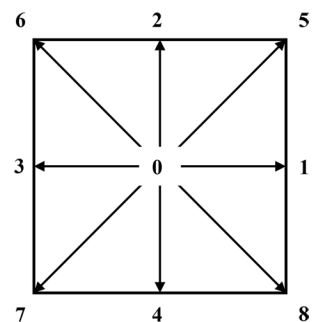
$$\eta_{act,an} = \varphi_{an,TPB} - \varphi_{ele,a,TPB}, \eta_{act,c} = \varphi_{ele,c,TPB} - \varphi_{ca,TPB} \tag{16}$$

where $\eta_{act,an}$ is the activation polarization voltage of anode, $\eta_{act,c}$ is the activation polarization voltage of cathode.

Finite-difference LBM for multicomponent flow

The relative molecular mass is different in the gas mixture. For example, the ratio of relative molecular weight between the H_2 and CO_2 is the largest which is 22. In order

Fig. 2 D_2Q_9 velocity model



to improve the LBM, the finite-difference LBM is used to simulate the mass transfer. The Boltzmann equation of every component is as follows [11],

$$\frac{\partial f^A}{\partial t} + \vec{\xi} \cdot \frac{\partial f^A}{\partial \vec{x}} + \vec{a} \cdot \frac{\partial f^A}{\partial \vec{\xi}} = J^{AA} + \sum J^{AB} \tag{17}$$

where f is the distribution function of gas species A, $\vec{\xi}$ is the velocity and \vec{a} is the acceleration, J^{AA} is the self-collision term which indicates the effect of collision between the same gas molecules, J^{AB} is the cross-collision term which indicates the effect of collision between the different gas molecules.

In the D₂Q₉ model, the gas molecular with smallest relative molecular mass has the fastest lattice speed which is given in the following equation [5],

$$c^A = \frac{\delta_x}{\delta_t} \tag{18}$$

$$\vec{e}_y = c^A \begin{cases} \vec{e}_0 = (0,0) & \vec{e}_1 = (1,0) & \vec{e}_2 = (-1,0) \\ \vec{e}_3 = (1,1) & \vec{e}_4 = (0,-1) & \vec{e}_5 = (1,1) \\ \vec{e}_6 = (1,-1) & \vec{e}_7 = (-1,-1) & \vec{e}_8 = (-1,1) \end{cases} \tag{19}$$

where c is the lattice speed of gas species A, δ_x is the streaming distance in the lattice unit, δ_t is the lattice time step, \vec{e}_y is the discrete velocity. The lattice velocities and discrete velocities of other gas molecules have the following form [11]:

$$c^B = \sqrt{\frac{M^A}{M^B}} c^A \tag{20}$$

$$\vec{e}_\alpha^B = c^B \cdot \vec{e}_\alpha^A \tag{21}$$

where B represents the other gas species. The speed of sound of each gas species is as follows,

$$c_{sp}^A = \frac{c^A}{\sqrt{3}}, c_{sp}^B = \frac{1}{\sqrt{3}} \sqrt{\frac{M^A}{M^B}} c^A \tag{22}$$

The Boltzmann equation of each gas species is discretized which is given in the following form,

$$\frac{\partial f_y^A}{\partial t} + \vec{e}_y^i \cdot \nabla f_y^A = J_y^{AA} + \sum J_y^{AB} + F_y^{\rightarrow A} \tag{23}$$

where

$$J_y^{AA} = -\frac{1}{\tau_f^A} (f_y^A - f_y^{A0}) \tag{24}$$

$$f_y^{A0} = \left[1 + \frac{1}{RT} (\vec{e}_y^{\rightarrow A} - \vec{u}_x) \cdot (\vec{u}^{\rightarrow A} - \vec{u}_x) \right] f_y^{A,eq} \tag{25}$$

$$f_y^{A,eq} = m_A \omega_y \left[1 + \frac{\vec{e}_y^{\rightarrow A} \cdot \vec{u}_m}{RT} + \frac{(\vec{e}_y^{\rightarrow A} \cdot \vec{u}_m)^2}{2(RT)^2} - \frac{u_m^{\rightarrow 2}}{2RT} \right] \tag{26}$$

$$J_y^{AB} = -\frac{1}{\tau_f^{AB}} \frac{m_B f_y^{A,eq}}{m_t} (\vec{e}_y^{\rightarrow A} - \vec{u}_m) \cdot (\vec{u}_A - u_B) \tag{27}$$

$$F_y^{\rightarrow A} = m_A \omega_y \frac{\vec{e}_y^{\rightarrow A} \cdot \vec{a}}{RT} \tag{28}$$

In the above equations, τ_f^A is the self-collision relaxation time, and τ_f^{AB} is the cross-collision relaxation time. The moments of the distribution function are used to obtain the concentration and speed of each gas species, and the equations are as following [27],

$$m_A = \sum_y f_y^A \tag{29}$$

$$\vec{u}_{yA} = \frac{\sum_y f_y^A \vec{e}_y^{\rightarrow A}}{m_A} \tag{30}$$

where m is the concentration of gas species A, \vec{u}_A is the velocity of gas species A. The concentration and velocity of gas mixture is calculated by the following equations.

$$m_t = \sum_A m_A \tag{31}$$

$$\vec{u}_m = \frac{\sum_A m_A \vec{u}_A}{m_t} \tag{32}$$

The finite-difference theory and LBM are coupled to improve the accuracy of simulation result. First, Eq. (23) is divided into two parts which are collision and streaming term, respectively. The equations are as follows.

$$\frac{\partial f_y^A}{\partial t} = J_y^{AA} + \sum J_y^{AB} + F_y^{\rightarrow A} \tag{33}$$

$$\frac{\partial f_y^A}{\partial t} = -e_y^{\rightarrow A} \cdot \nabla f_y^A \quad (34)$$

The explicit first-order Euler scheme is adopted to discretize Eq. (33).

$$f_y^{A+} = f_y^A + \delta_t J_y^{AA} + \delta_t J_y^{AB} + \delta_t F_y^{\rightarrow A} \quad (35)$$

Equation (34) is discretized by a second-order Lax-Wendroff scheme which is given in the following equation.

$$f_y^A(\vec{x}, t + \delta_t) = f_y^{A+}(\vec{x}, t) - \delta_t (e_y^{\rightarrow A} \cdot \nabla) f_y^{A+}(\vec{x}, t) + \frac{1}{2} \delta_t^2 (e_y^{\rightarrow A} \cdot \nabla)^2 f_y^{A+}(\vec{x}, t) \quad (36)$$

Concentration and ohmic polarization model

Due to the concentration difference, the polarization loss is described as follows [33],

$$\eta_{con_a} = -\frac{RT}{2F} \ln\left(\frac{\gamma_{H_2,TPB} \gamma_{H_2O,initial}}{\gamma_{H_2,initial} \gamma_{H_2O,TPB}}\right) \quad (37)$$

$$\eta_{con_c} = -\frac{RT}{2F} \ln\left(\frac{\gamma_{O_2,TPB}}{\gamma_{O_2,initial}}\right)^{\frac{1}{2}} \quad (38)$$

where η_{con_a} is the concentration polarization voltage of anode, η_{con_c} is the concentration polarization voltage of cathode, γ is the molar fraction.

In order to establish the comprehensive simulation model of SOFC, the ohm's law is used to calculate the ohmic polarization. Because there is the higher electron conductivity of the electrode, the ohmic loss of the electrode is ignored [28–31]. Equation (42) is used to calculate the ohmic polarization voltage of electrolyte [32].

$$\eta_{ohm} = i_{TPB} \sum O_e \quad (39)$$

where η_{ohm} is the ohmic polarization voltage of SOFC, O_e is the ohmic resistance of electrolyte, anode, and cathode.

Boundary conditions

In the charge transport model, the input boundaries of anode and cathode are given in the following form [1],

$$\varphi_{in,a} = E_{theory} \varphi_{in,c} = 0 \quad (40)$$

where E_{theory} is the theory potential. The equations of top and bottom boundary are as follows [1],

$$\frac{\partial \varphi}{\partial y} = 0 \quad (41)$$

At the TPB, the current density is continuous which can be described as follows [1],

$$\sigma_{an} \nabla \varphi_{TPB,an} = \sigma_{ca} \nabla \varphi_{TPB,c} \quad (42)$$

where σ is the electrical conductivity.

As shown in Fig. 1, the total concentrations of external syngas and air are specified at the input of anode and cathode. At the TPB, the mass flux is specified using Eq. (11). As for the top and bottom boundary, the periodic boundary is employed [34–38].

Model validation

The model validation consists of two parts. Firstly, the characteristics of SOFC voltage-current between the numerical model and specific experimental setups are compared. Secondly, the relative error between the simulation and measured values is calculated. The model validation and subsequent simulation experiments are conducted by means of MATLAB.

Other parameters for planar anode-supported SOFC are listed in Table 1 [41, 42].

The comparison between the simulated and measured values is shown in Fig. 3, where the gas mixture only contains H₂ and H₂O. The initial molar fractions of two components are 0.97 and 0.03, respectively [39, 40]. In Fig. 3, it is found that the simulation data closely overlaps with the experimental data. When the current density is 0.75 A cm⁻², the experimental and simulation data are 0.6775 V and 0.64755 V, respectively, and the voltage difference is largest. Figure 3 also depicts the relative error between the simulated and measured values. The maximum relative error is about 4.42%, implying that this numerical model can accurately simulate the operation progress of SOFC.

Result and analysis

In order to investigate the operation mechanism of SOFC fueled with external syngas, the effect of operation and structure parameters on performance of SOFC is discussed.

Effect of external syngas on performance of SOFC

In the direct reforming experiment, the gas mixture includes the CH₄ and H₂O, with component ratios of 0.97 and 0.03 [31], respectively. The initial component ratios of external syngas for H₂, H₂O, CH₄, CO, and CO₂ are 0.263, 0.493,

Table 1 Input parameters used in the standard case and model validation

Parameter	Symbol	Unit	Value
Operation temperature	T	K	1023
Operation pressure	p	pa, gauge pressure	101,325
Anode porosity	ϵ_a	%	5
Cathode porosity	ϵ_c	%	5
Anode thickness	d_a	m	1.05×10^{-3}
Cathode thickness	d_c	m	5×10^{-5}
Electrolyte thickness	d_e	m	5×10^{-5}
Permeability of anode	$K_{_a}$	m^{-2}	1.76×10^{-11}
Permeability of cathode	$K_{_c}$	m^{-2}	2.33×10^{-11}
For model validation (Anode)	Symbol	Unit	Value
Mixture concentration at inlet	$C_{t,a}$	$\text{mol}\cdot\text{m}^{-3}$	11.3
Activation energy for anode	$E_{_a}$	$\text{J}\cdot\text{mol}^{-1}$	1.4×10^5
Pre-exponential factor of anode	$A_{_a}$	$\text{A}\cdot\text{m}^{-2}$	6.54×10^{11}
For model validation (Cathode)	Symbol	Unit	Value
Air concentration at inlet	$C_{t,c}$	$\text{mol}\cdot\text{m}^{-3}$	22.6
Activation energy for cathode	$E_{_c}$	$\text{J}\cdot\text{mol}^{-1}$	1.37×10^5
Pre-exponential factor of cathode	$A_{_c}$	$\text{A}\cdot\text{m}^{-2}$	2.35×10^{11}
N ₂ mole fraction at inlet	γ_{1c}	%	79
O ₂ mole fraction at inlet	γ_{2c}	%	21

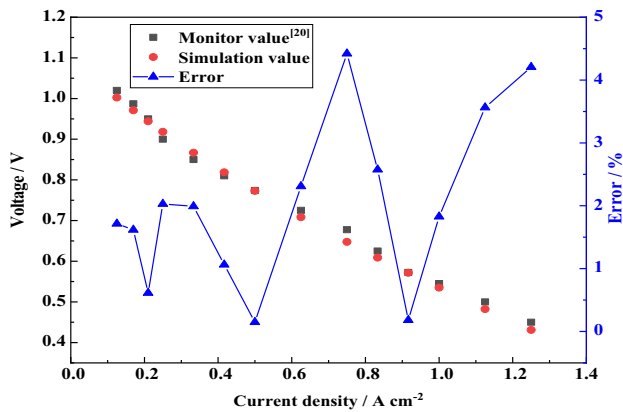


Fig. 3 Comparison of volt-ampere characteristics between the experimental data [20] and predictions values by the present model with two components

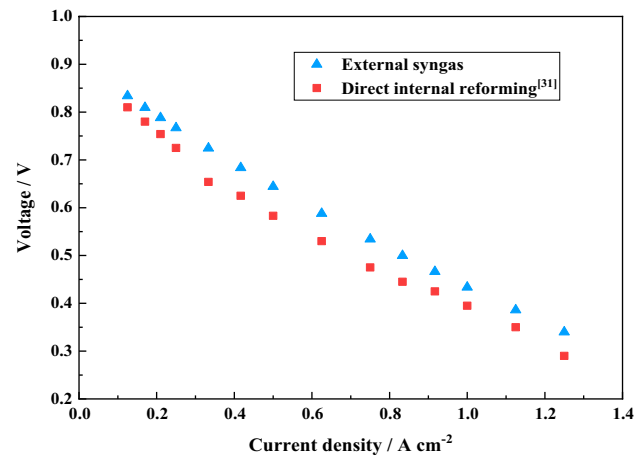


Fig. 4 Comparison of output voltage with different current densities with gas mixture H₂O and CH₄ [31] and external syngas

0.171, 0.029, and 0.044, respectively [40–43]. The simulation of performance with five components is performed, as is shown in Fig. 4. The voltage difference range is larger when the current density is from 0.33 A cm⁻² to 0.75 A cm⁻², about from 0.0577 V to 0.07 V. In comparison to supplied with the gas mixture of H₂O and H₂, the output voltage of SOFC supplied with the gas mixture of H₂O and CH₄ and the external syngas degrades. But compared to supplied with the gas mixture of H₂O and CH₄, the output voltage of SOFC supplied with the external syngas is higher. One of the possible reasons is that due to the existence of MRS and WGS, the partial chemical energy will be consumed during the

direct internal reforming, which results in the decrease of chemical energy converting into electric potential. Meanwhile, the MRS and WGS processes are endothermic reactions leading to the lower performance of SOFC. Another reason may be that there is more H₂ present in the external syngas than a gas mixture of H₂O and CH₄. More H₂ can arrive at the TPB, which can reduce the effect of concentration polarization. Thus, the use of external syngas can enhance the performance of SOFC.

Owing to the existence of reforming reaction, the component ratio of CH₄ plays a core role on the performance of SOFC. The effect of CH₄ molar fraction on the concentration

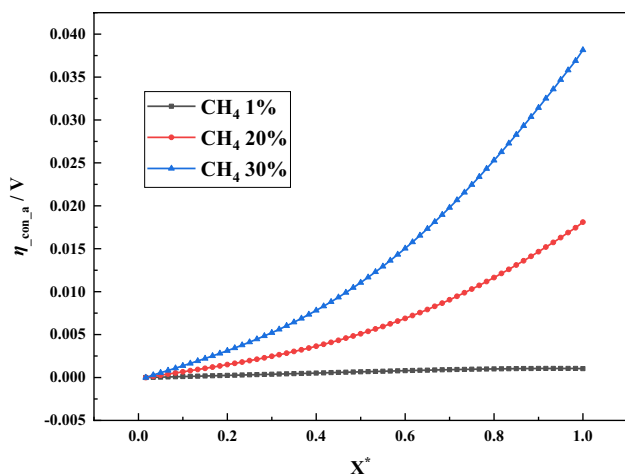


Fig. 5 Effect of component ratio of CH₄ on the performance of SOFC

overpotential is shown in Fig. 5. The X-axis in Fig. 5 is along the thickness of porous electrode, which have been normalized. The equation is as follow,

$$X^* = \frac{x}{d} \quad (43)$$

where x is the distance between the inlet of porous electrode and calculation point, d is the thickness of porous electrode.

When the component ratio of CH₄ is 30%, the concentration overpotential is maximum at the TPB, about 0.0382 V. With the increment of initial molar fraction, the concentration overpotential becomes larger. Because the loss of reactant will cause the output voltage to be lower than the theoretical voltage at the specific current density. By changing the molar fraction of CH₄, the concentration of H₂ will decrease. To meet the output power, the CH₄ is consumed to

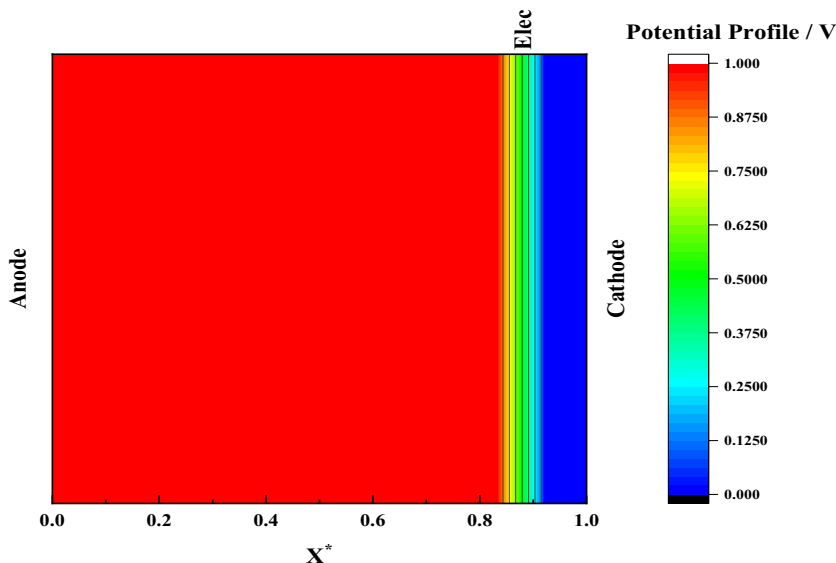
generate more H₂. Nevertheless, the reaction rate of reforming is lower, which makes it difficult to meet the consumption of H₂, leading to the higher concentration polarization voltage. In Fig. 5, it is found that the lower molar fraction of CH₄ is beneficial for improving the performance of SOFC.

Effect of electro conductivity

Figure 6 illustrates the potential distribution of SOFC, which clearly demonstrates that the potential drops in both the anode and cathode are minimal. In the electrolyte, the potential drop ranges from 0.943 V to 0.115 V. Additionally, the potential drops across the anode and cathode are approximately 0.002 V and 0.004 V. The potential difference at the interface between the anode and electrolyte measures 0.054 V, while the potential difference at the interface between the electrolyte and cathode is significantly larger, approximately 0.1112 V. The different materials of the electrolyte, the porous anode and the porous cathode leads to different electro conductivities, which results in the potential difference in the interface between electrodes and electrolyte. In Fig. 6, there is a rapid potential drop in the electrolyte because of lower conductivity compared to the anode and cathode. There are larger potential differences at the interfaces, particularly at the interface between the electrolyte and cathode. It is beneficial to decrease the potential difference at the interface by improving the electrolyte conductivity.

Figure 7 depicts the effect of electro conductivity of electrolyte on the electrochemical reaction. It is found in Fig. 7 that the reaction current density at the TPB increases with the increment of electro conductivity. At the middle region of TPB, the current density is lower. Especially, the minimum current density is about 3583.94 A m⁻² when the

Fig. 6 Distribution of potential at the representative surface element scale of SOFC



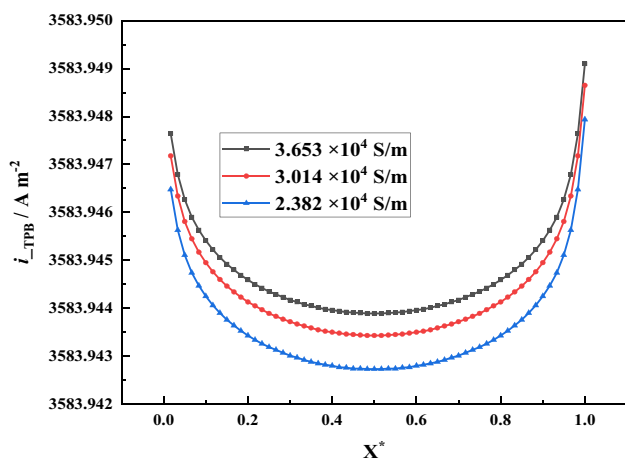


Fig. 7 Effect of electron conductivity on electrochemical performance of anode

Table 2 Initial molar fractions of external syngas used in the standard case

Parameter	Symbol	Unit	Value
CH ₄ mole fraction at inlet	γ_{1a}	-	0.01
H ₂ mole fraction at inlet	γ_{2a}	-	0.4
H ₂ O mole fraction at inlet	γ_{3a}	-	0.4
CO mole fraction at inlet	γ_{4a}	-	0.1
CO ₂ mole fraction at inlet	γ_{5a}	-	0.09

electro conductivity is $2.382 \times 10^4 \text{ S m}^{-1}$. As the electro conductivity becomes larger, the performance of charge transport will become better, which can also promote the electrochemical reaction rate at the TPB. Nevertheless, the voltage difference will become larger by increasing the electro conductivity of the anode/cathode. Now, it is more difficult to improve the performance of charge transport for the electrolyte by decreasing the thickness of electrolyte during the manufacturing process. Thus, there are the technological barriers for the novel material of electrolyte.

Standard case

The initial component ratios of external syngas are reset, which is shown in Table 2.

Figure 8 demonstrates the change of five components in the standard case. The molar fractions of CH₄, CO, and H₂ all decrease along the direction of gas mixture flow, while the molar fractions of CO₂ and H₂O increase. At the TPB, the molar fraction of CH₄, H₂, H₂O, CO₂ and CO are about 0.00804, 0.37997, 0.41601, 0.11867 and 0.07731, respectively. The maximum concentration overpotential is about 0.00419.

In the standard case, the simulation results for the cathode, including the concentration polarization and the molar fractions of N₂ and O₂ along the gas flow direction, are shown in Fig. 9. The maximum of concentration overpotential is about $1.3 \times 10^{-4} \text{ V}$ and the minimum of O₂ molar fraction is about 0.2074. Because the supplied gas is usually excessive in the cathode, the effect of concentration polarization is lower.

Parametric analysis of anode

Several other key parameters also significantly influence mass transfer, including total concentration of external syngas, operation temperature and thickness of anode.

Effect of gas mixture concentration

The effect of total concentration of external syngas on mass transfer is shown in Fig. 10. By analyzing the curve of five components along the gas flowing, it can be found that the molar fractions of the CH₄, CO and H₂ all increase with the increment of total concentration. The mole fractions of the H₂O and CO₂ become lower by increasing the total concentration. Moreover, the concentration overpotential becomes lower with the increment of total concentration. The consumption of H₂ and the concentration overpotential are two important parameters of simulations. When the total gas mixture concentration is $9 \text{ mol} \cdot \text{m}^{-3}$, the H₂ molar fraction and concentration overpotential are about 0.3746 V and $5.321 \times 10^{-3} \text{ V}$ at TPB. The molar fraction of CO changes from 0.1 to 0.07, indicating that the consumption of CO is also larger.

As the external syngas concentration increases, a greater number of reactant gas molecules can flow into the TPB, enhancing the potential for participation in both chemical and electrochemical reactions. Simultaneously, the concentration difference between the inlet and TPB decreases with the increasing gas mixture concentration. However, the total concentration of the gas mixture cannot be added without restrictions, which will cause the waste of reactant gas leading to the lower working efficiency of SOFC.

Effect of anode temperature

The influence of operation temperature on mass transfer is illustrated in Fig. 11. With the increment of the operation temperature, there are significant changes about the molar fractions of CH₄, H₂ and H₂O. For example, when the operation temperature is 1073 K, the molar fractions of CH₄, H₂ and H₂O are about 0.0076, 0.336 and 0.465 at the TPB. The variations of another two gases are insignificant by increasing the operation temperature.

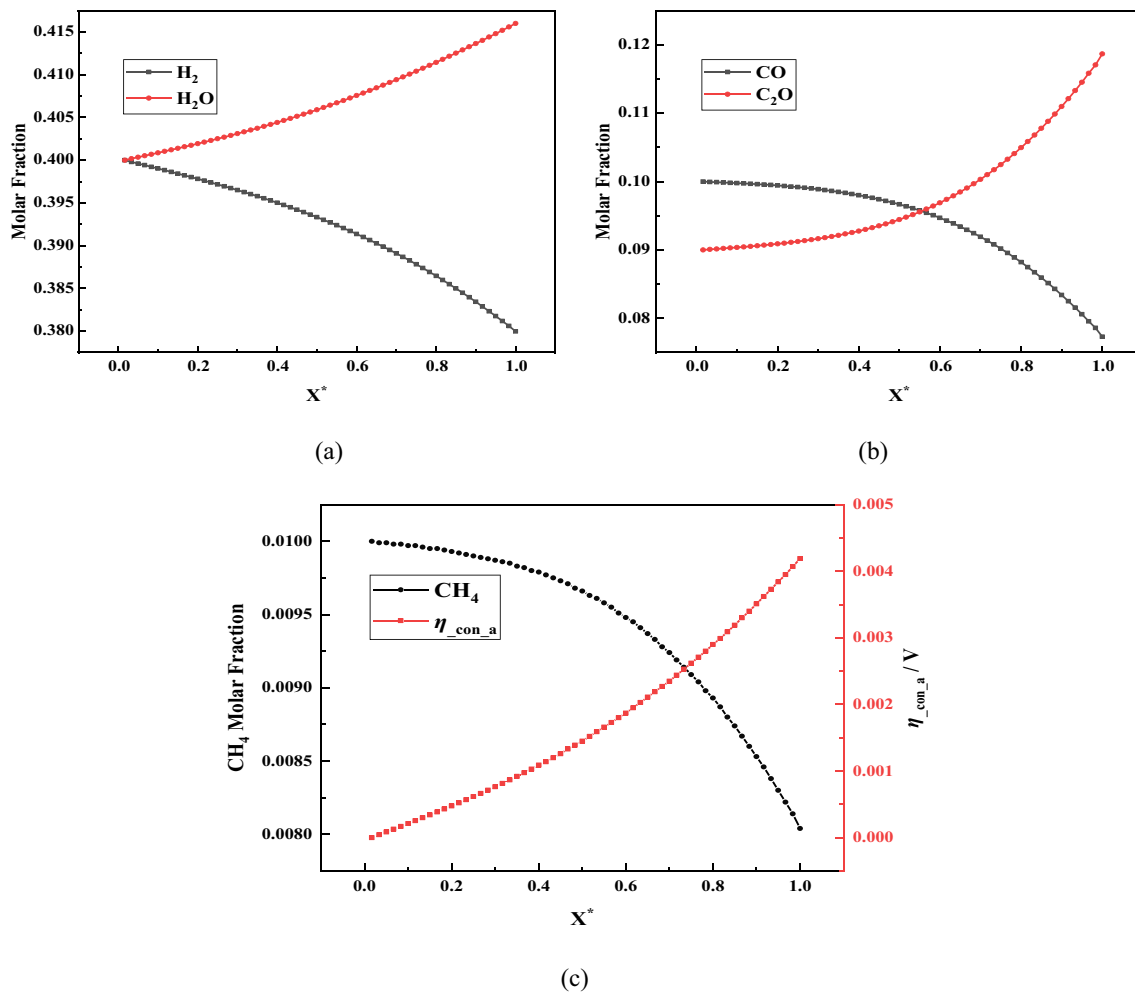
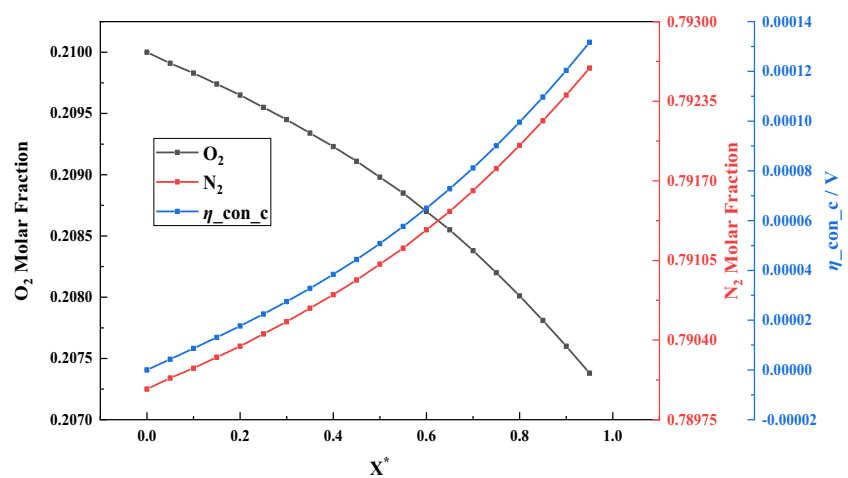


Fig. 8 A) Distribution of H_2 and H_2O along the gas flowing in the standard case; (b) Distribution of CO and COO along the gas flowing in the standard case; (c) Distribution of CH_4 and concentration polarization voltage along the gas flowing in the standard case

Fig. 9 Change curves of cathode gas molar fraction and concentration overpotential in the standard case



The possible reason is that the temperature requirements for different chemical reactions are different. By increasing the temperature, the electrochemical reaction rates between

H_2 and O_2 become larger, consuming more H_2 and producing more H_2O . At higher temperature, the reforming reaction of CH_4 is intense, which results in the molar fraction drop of

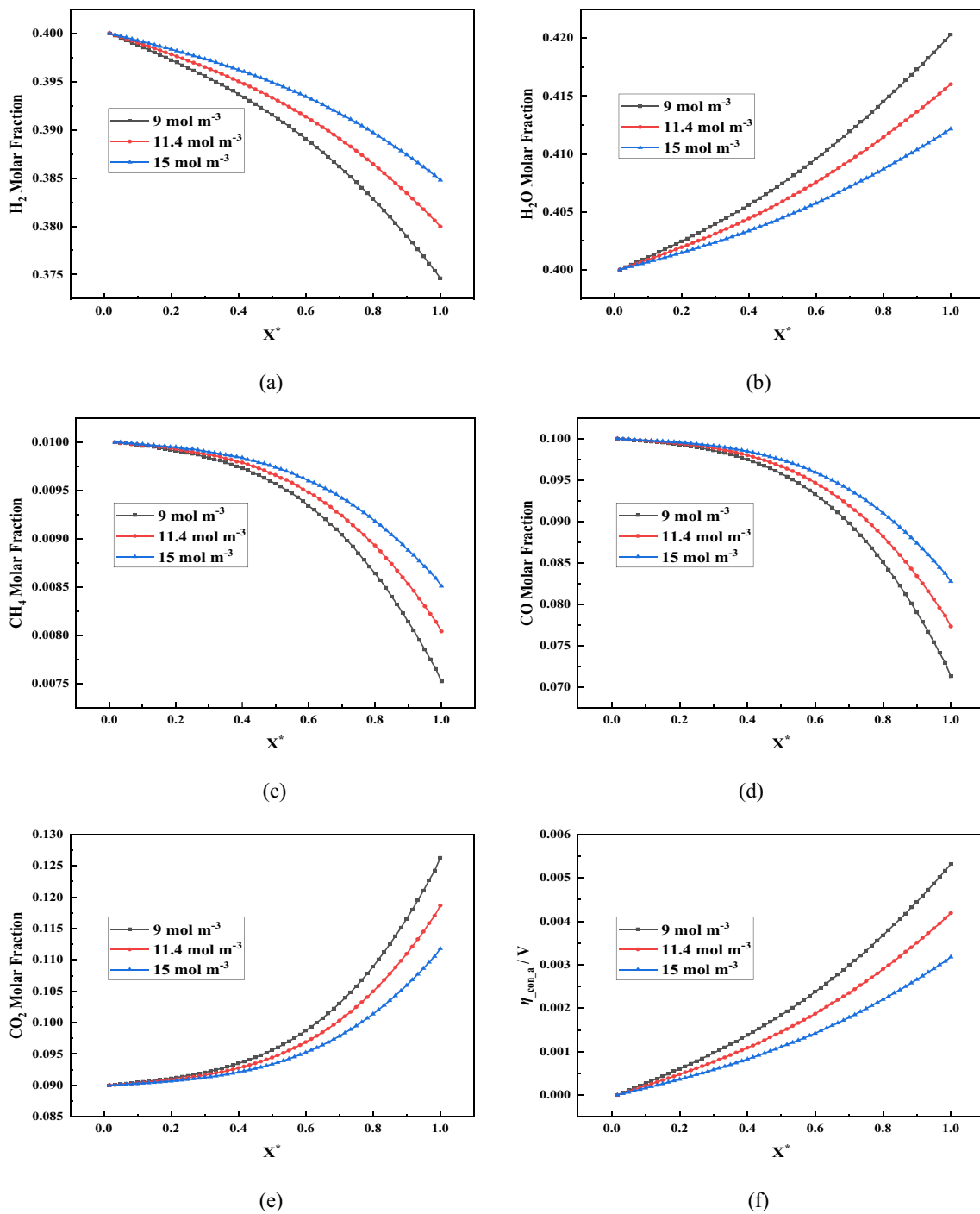


Fig. 10 Effect of total concentration on the distributions of five components and performance of anode

CH_4 with the increase of temperature. The chemical reaction between CO and H_2O can take place at the lower temperature (< 973 K). Thus, the effect of increasing temperature on the chemical reaction is insignificant. However, at the higher temperature, the solid particles with catalysis may drop, leading to the decrease of SOFC performance. The temperature of SOFC cannot also be increased without limitations,

because the thermal management plays an important role on the maintaining the output voltage of SOFC.

Effect of anode thickness

The effect of anode thickness on the concentration overpotential is shown in Fig. 12. When the thickness

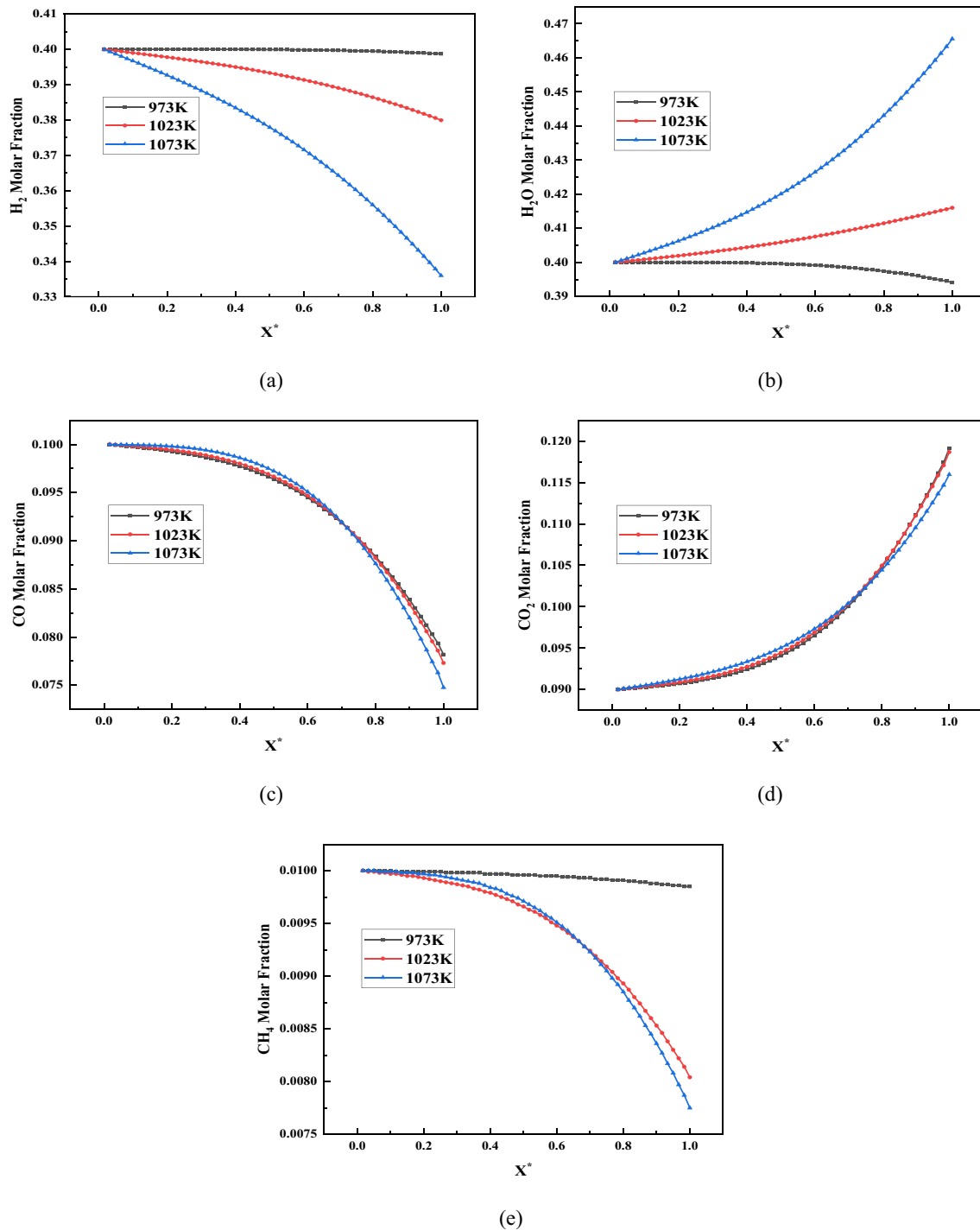


Fig. 11 Effect of temperature on the distributions of five components in the anode

of anode becomes larger, the concentration overpotential increases. The concentration polarization voltage is 0.038 V when the anode thickness is 1.55 mm. The main reason is that the resistance flowing along the horizontal direction becomes larger by increasing the anode thickness. Compared to increasing the anode thickness, the

change of performance of SOFC is less by decreasing the thickness of anode although the resistance of gases flowing becomes lower.

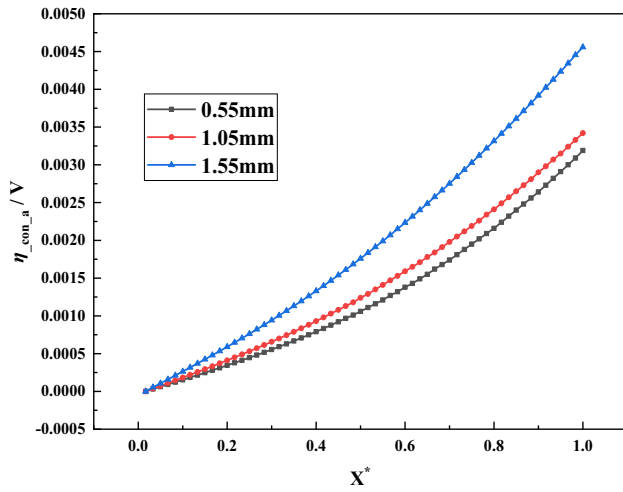


Fig. 12 Effect of anode thickness on the performance in the anode

Parametric analysis of cathode

In the cathode, the electrochemical reaction is simpler compared to the anode. Two main parameters are explored, namely the operation temperature and thickness of anode.

Effect of temperature

The simulation results at different temperatures are described in Fig. 13, which illustrate that the consumption of O_2 becomes larger and the component ratio of N_2 increases by improving the temperature. The concentration polarization voltage increases with the increment of temperature. When the operation temperature is 1073 K, the molar fraction and concentration overpotential of cathode are about 0.1992×10^{-4} V and 5.558×10^{-4} V. The main reason is that it is useful to improve the electrochemical reaction rate between the H_2 and O_2 by increasing the temperature. In Fig. 13, it is also found that the effect of changing the operation temperature from 1023 to 1073 K on the mass transfer

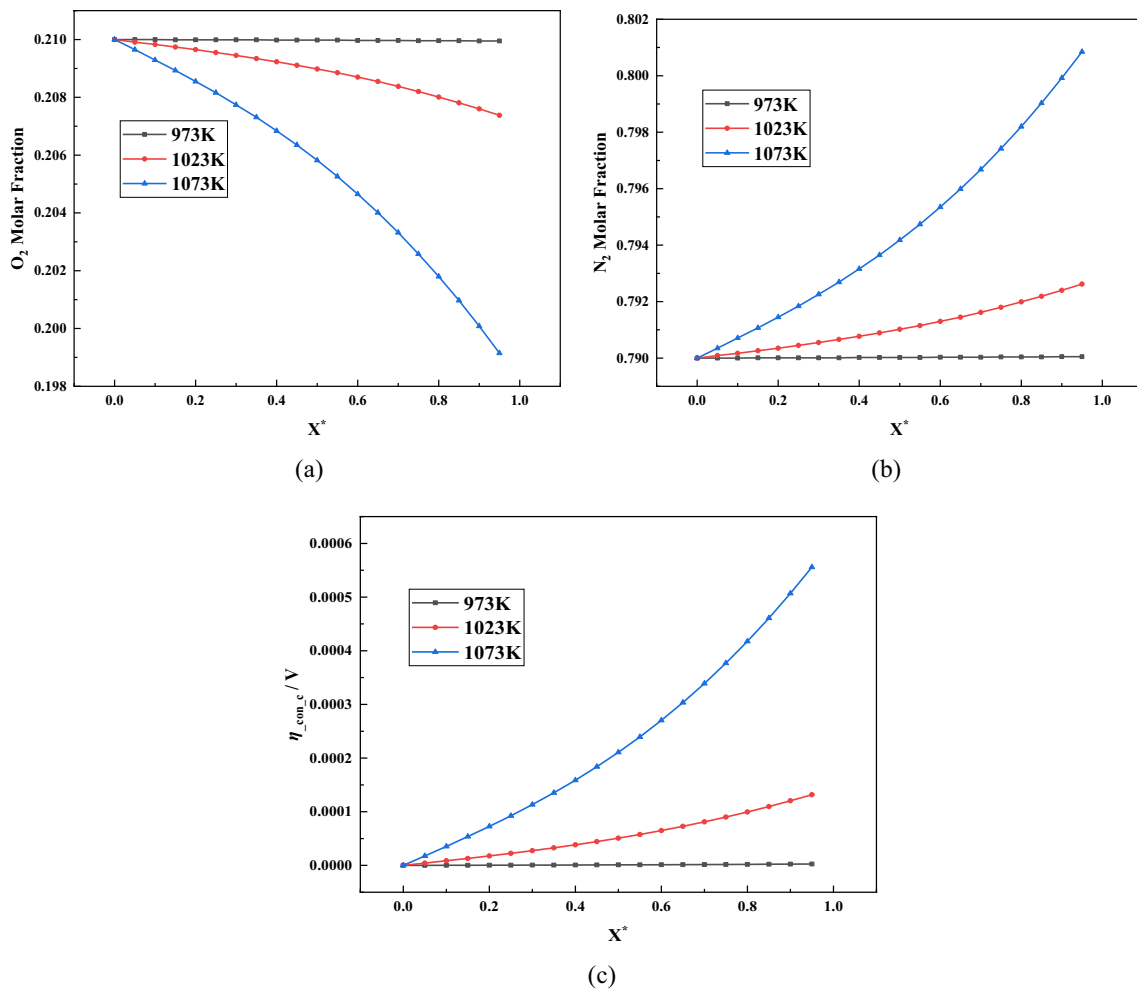


Fig. 13 Effect of temperature on the distributions of two components and concentration polarization voltage in the cathode

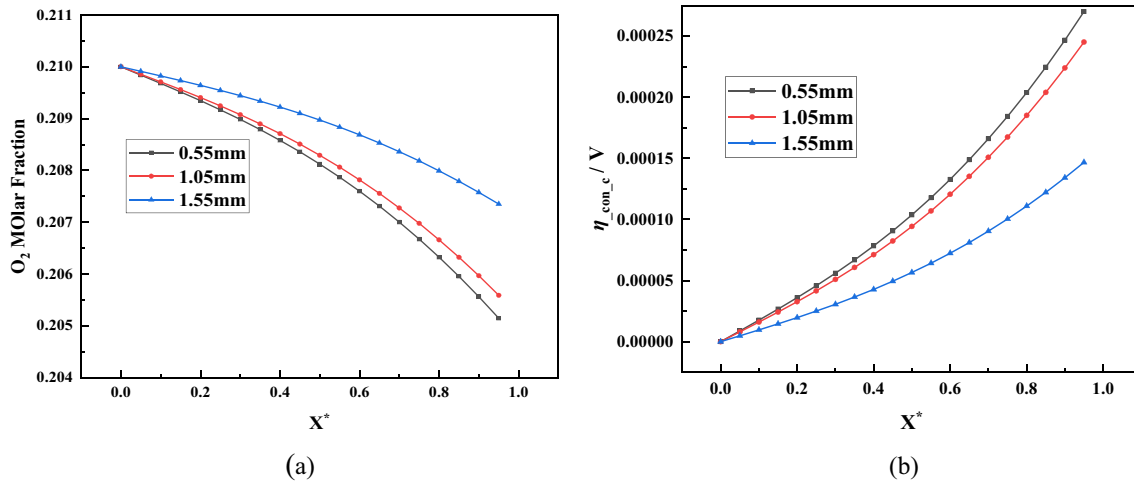


Fig. 14 Effects of anode thickness on the mass transport and electrochemical reaction of cathode

is more significant. The possible reason is that the electrochemical reaction between H₂ and O₂ is close to the theory ideal state at 1073 K.

Effect of anode thickness on mass transport of cathode

Figure 14 describes the effect of increasing the anode thickness on the mass transfer in the cathode. By adjusting the thickness of anode, there is a change in the consumption of O₂. When the anode thicknesses are 0.55 mm, 1.05 mm and 1.55 mm, the concentration overpotentials are 2.702×10^{-4} V, 2.452×10^{-4} V and 1.467×10^{-4} V, respectively. In Fig. 14, it is found that the consumption of O₂ and the concentration overpotential of cathode both decreases with the increase of anode thickness. It is because that the resistance of gases flow in the anode becomes larger with the increasing of thickness, resulting in the decrease of reactant gas molecular quantity at the TPB of anode. The consumption of O²⁻ and the consumption of O₂ both decreases in the anode, leading to the drop of concentration polarization voltage. The change of operation performance in the cathode should be considered if the researchers want to improve the performance of SOFC by employing the strategy of adjusting the anode thickness.

Conclusions

To gain a deeper understanding of the multi-physics fields coupling in SOFC fueled by external syngas, a comprehensive numerical model for SOFC is designed and validated. In this model, the charge transport and mass transfer are simulated based on the REV scale LBM and the finite-difference LBM, respectively. Based on the parameter analysis of SOFC, some important conclusions are as follows:

- (1) The multi-physics fields coupling model is useful to predict the gas components, potential and polarization loss distributions in the SOFC.
- (2) Due to the low electric conductivity, there is a significant drop in electrostatic potential within the electrolyte, and increasing conductivity of electrolyte is beneficial for improving the electrochemical reaction rate.
- (3) Compared to the gas mixture of H₂O and CH₄, supplying the external syngas to the anode helps to improve the performance of SOFC. To enhance the output voltage of SOFC, the CH₄ component ratio should be controlled within a lower range, which is less than 0.2.
- (4) By increasing the concentration of the external syngas, the concentration polarization decreases. However, the consumption of H₂ and production of H₂O will become larger by increasing the temperature, which results in a decrease in the performance of SOFC.
- (5) The gas transfers in both the cathode and anode are influenced by changing the anode thickness. The consumption of O₂ decreases with an increase of anode thickness.

Findings

This study was funded by the National Natural Science Foundation of China (Grant nos. 52276026, 52006136) and Fundamental Research Funds for the Central Universities (2023JBMC016).

Nomenclature

a Acceleration (m·s.⁻²)

c	Lattice sound speed ($\text{m}\cdot\text{s}^{-1}$)
E_{theory}	Theory potential (V)
e	Discrete lattice velocity
F	Faraday constant ($96,485 \text{ A}\cdot\text{s}\cdot\text{mol}^{-1}$)
f	Lattice Boltzmann distribution function
I	Mass flux ($\text{kg}\cdot\text{m}^{-2}\cdot\text{s}^{-1}$)
i	Current density ($\text{A}\cdot\text{m}^{-2}$)
J	Collision term
j	Molar flux ($\text{mol}\cdot\text{m}^{-2}\cdot\text{s}^{-1}$)
k	Reaction coefficient ($\text{mol}\cdot\text{m}^{-3}\cdot\text{Pa}^{-2}\cdot\text{s}^{-1}$)
M	Molecular weight ($\text{kg}\cdot\text{mol}^{-1}$)
m	Lattice molar concentration of gas
n	Electronic exchange coefficient
O	Ohmic resistance (Ω)
Q	External force term
p	Pressure (pa)
R	Universal gas constant ($8.314 \text{ J}\cdot\text{mol}^{-1}\cdot\text{K}^{-1}$)
S	Source term
T	Operation temperature (K)
t	Time (s)
u	Velocity of gas ($\text{m}\cdot\text{s}^{-1}$)
x	Coordinate along the direction of electrode thickness

Greek symbols

γ	Molar fraction
ν	Kinematic viscosity ($\text{m}^2\cdot\text{s}^{-1}$)

φ	Electrostatic potential (V)
η	Polarization voltage (V)
τ	Relaxation time
α	Transfer coefficient
ξ	Lattice velocity of gas ($\text{m}\cdot\text{s}^{-1}$)

Author contributions The statements of author contributions are as follows:

Yongqi Wei: Writing and Editing, Methodology, Software, Investigation, Writing original draft preparation, Data curation;
Zhi Ning: Investigation and Validation, Investigation.
Chunhua Sun: Editing, Data curation, Writing-Reviewing.
Ming Lv: Investigation.
Yechang Liu: Investigation.
All authors reviewed the manuscript.

Data availability No datasets were generated or analysed during the current study.

Declarations

Competing interests The authors declare no competing interests.

Ethical approval This declaration is not applicable.

References

- Xu H, Chen Y, Kim J H, Dang Z, Liu M (2019) Lattice Boltzmann modelling of the coupling between charge transport and electrochemical reactions in a solid oxide fuel cell with a patterned anode [J]. *Int J Hydrogen Energy* 44(57):30293–30305. <https://doi.org/10.1016/j.ijhydene.2019.09.086>
- Park YM, Lee HJ, Bae HY et al (2012) Effect of anode thickness on impedance response of anode-supported solid oxide fuel cells [J]. *Int J Hydrogen Energy* 37(5):4394–4400. <https://doi.org/10.1016/j.ijhydene.2011.11.152>
- Grew KN, Joshi AS, Peracchio AA, Chiu WKS (2012). Pore-scale investigation of mass transport and electrochemistry in a solid oxide fuel cell anode [J]. *J Power Sources* 195:2331–2345. <https://doi.org/10.1016/j.jpowsour.2009.10.067>
- Joshi AS, Peracchio AA, Grew KN, Chiu WKS (2007) Lattice Boltzmann method for multi-component, non-continuum mass diffusion [J]. *J Phys D Appl Phys* 40:7593–7600. <https://doi.org/10.1088/0022-3727/40/23/053>
- Joshi A S, Grew K N, Peracchio A A, Chiu WKS (2007). Lattice Boltzmann modeling of 2D gas transport in a solid oxide fuel cell anode [J]. *J Power Sources* 164(2):631–638. <https://doi.org/10.1016/j.jpowsour.2006.10.101>
- Chan SH, Khor KA, Xia ZT (2001) A complete polarization model of a solid oxide fuel cell and its sensitivity to the change of cell component thickness [J]. *J Power Sources* 93(1–2):130–140. [https://doi.org/10.1016/s0378-7753\(00\)00556-5](https://doi.org/10.1016/s0378-7753(00)00556-5)

7. Kasra Nikooyeh, Ayodeji A. Jeje, Josephine M, Hill (2007). 3D modeling of anode-supported planar SOFC with internal reforming of methane [J]. *J Power Sources* 171(2):601–609. <https://doi.org/10.1016/j.jpowsour.2007.07.003>
8. Meng N (2012) Modeling of SOFC running on partially pre-reformed gas mixture [J]. *Int J Hydrogen Energy* 37(2):1731–1745. <https://doi.org/10.1016/j.ijhydene.2011.10.042>
9. Grew KN, Joshi AS, Peracchio AA et al (2006) Detailed electrochemistry and gas transport in a SOFC anode using the lattice Boltzmann method [C]. ASME 2006 International Mechanical Engineering Congress and Exposition. Advanced Energy Systems, Chicago, pp.285–290. <https://doi.org/10.1115/IMECE2006-13621>
10. Xu H, Dang Z, Bai BF (2012) Numerical simulation of multispecies mass transfer in a SOFC electrodes layer using lattice Boltzmann method [J]. *J Fuel Cell Sci Technol* 9(6):061004-. <https://doi.org/10.1115/1.4007791>
11. Dang Z, Xu H (2016) Pore scale investigation of gaseous mixture flow in porous anode of solid oxide fuel cell [J]. *Energy* 107:295–304. <https://doi.org/10.1016/j.energy.2016.04.015>
12. Xu H, Dang Z, Bai BF (2014) Electrochemical performance study of solid oxide fuel cell using lattice Boltzmann method [J]. *Energy* 67:575–583. <https://doi.org/10.1016/j.energy.2014.02.021>
13. Yakabe H, Hishinuma M, Uratani M, Matsuzaki Y, Yasuda I (2000). Evaluation and modeling of performance of anode-supported solid oxide fuel cell [J]. *J Power Sources* 86(1–2):423–431. [https://doi.org/10.1016/s0378-7753\(99\)00444-9](https://doi.org/10.1016/s0378-7753(99)00444-9)
14. Yan M, Zeng M, Chen QY, Wang QW (2012) Numerical study on carbon deposition of SOFC with unsteady state variation of porosity [J]. *Appl Energy* 97:754–762. <https://doi.org/10.1016/j.apenergy.2012.02.055>
15. Baldinelli A, Barelli L, Bidini G (2015) Performance characterization and modelling of syngas-fed SOFCs (solid oxide fuel cells) varying fuel composition [J]. *Energy* 90(2):2070–2084. <https://doi.org/10.1016/j.energy.2015.07.126>
16. Ni M, Leung MKH, Leung DYC (2007) Parametric study of solid oxide fuel cell performance [J]. *Energy Convers Manage* 48(5):1525–1535. <https://doi.org/10.1016/j.enconman.2006.11.016>
17. Pramuanjaroenkij A, Kakac S, Zhou X (2008). Mathematical analysis of planar solid oxide fuel cells [J]. *Int J Hydrogen Energy* 33(10):2547–2565. <https://doi.org/10.1016/j.ijhydene.2008.02.043>
18. Ebbesen SD, Knibbe R, Mogensen M (2012) Co-electrolysis of steam and carbon dioxide in solid oxide cells [J]. *J Electrochem Soc* 159(8):482–9. <https://doi.org/10.1149/2.076208jes>
19. Kazempoor P, Braun RJ (2014) Model validation and performance analysis of regenerative solid oxide cells for energy storage applications: Reversible operation [J]. *Int J Hydrogen Energy* 39(11):5955–71. <https://doi.org/10.1016/j.ijhydene.2014.01.186>
20. Delavar MA, Farhadi M, Sedighi K (2010) Numerical simulation of direct methanol fuel cells using lattice Boltzmann method [J]. *Int J Hydrogen Energy* 35(17):9306–9317. <https://doi.org/10.1016/j.ijhydene.2010.02.126>
21. Guo Z, Zheng C, Shi B (2002) Discrete lattice effects on the forcing term in the lattice Boltzmann method [J]. *Phys Review E* 65(4):046308-. <https://doi.org/10.1103/PhysRevE.65.046308>
22. Shan X, Doolen G (1996). Diffusion in a multicomponent lattice Boltzmann equation model [J]. *Phys Rev E* 54(4):3614–3620. <https://doi.org/10.1103/PhysRevE.54.3614>
23. Yahya A, Naji H, Dhahri H (2022) A lattice Boltzmann analysis of the performance and mass transport of a solid oxide fuel cell with a partially obstructed anode flow channel [J]. *Fuel* 334(1):126537. <https://doi.org/10.1016/j.fuel.2022.126537>
24. Guo Z (2002). Lattice Boltzmann model for incompressible flows through porous media [J]. *Phys Rev E* 66(3):36304-. <https://doi.org/10.1103/physreve.66.036304>
25. Zhao F, Armstrong TJ, Virkar AV (2003) Measurement of O₂-N₂ effective diffusivity in porous media at high temperatures using electrochemical cell [J]. *J Electrochem Soc* 150(3):249–56. <https://doi.org/10.1149/1.1540156>
26. Chiu WKS, Joshi AS, Grew KN (2009) Lattice Boltzmann model for multi-component mass transfer in a solid oxide fuel cell anode with heterogeneous internal reformation and electrochemistry [J]. *Eur Phys J Spec Top* 171(1):159–165. <https://doi.org/10.1140/epjst/e2009-01024-8>
27. Zou QS, He XY (1997) On pressure and velocity boundary conditions for the lattice Boltzmann BGK model [J]. *Phys Fluids* 9(6):1591–0. <https://doi.org/10.1063/1.869307>
28. Blesznowski M, Sikora M, Kupecki J, Makowski L, Orciuch W (2022) Mathematical approaches to modelling the mass transfer process in solid oxide fuel cell anode [J]. *Energy* 239:121878. <https://doi.org/10.1016/j.energy.2021.121878>
29. Grew KN, Chiu WKS (2012). A review of modeling and simulation techniques across the length scales for the solid oxide fuel cell [J]. *J Power Sources* 199:1–13. <https://doi.org/10.1016/j.jpowsour.2011.10.010>
30. Chan SH, Khor KA, Xia ZT (2001) A complete polarization model of a solid oxide fuel cell and its sensitivity to the change of cell component thickness [J]. *J Power Sources* 93(1–2):130–140. [https://doi.org/10.1016/s0378-7753\(00\)00556-5](https://doi.org/10.1016/s0378-7753(00)00556-5)
31. Xie Y, Ding H, Xue X (2013) Multi-physicochemical modeling of direct methane fueled solid oxide fuel cells [J]. *J Power Sources* 241:718–27. <https://doi.org/10.1016/j.jpowsour.2013.06.028>
32. Guo Z, Zheng C, Shi B (2002) Non-equilibrium extrapolation method for velocity and pressure boundary conditions in the lattice Boltzmann method [J]. *Chin Phys* 11(4):366–374. <https://doi.org/10.1088/1009-1963/11/4/310>
33. Zhao F, Virkar AV (2005) Dependence of polarization in anode-supported solid oxide fuel cells on various cell parameters [J]. *J Power Sources* 141(1):79–95. <https://doi.org/10.1016/j.jpowsour.2004.08.057>
34. Joshi AS, Peracchio AA, Grew KN, Chiu WKS (2007) Lattice Boltzmann method for continuum, multi-component mass diffusion in complex 2D geometries [J]. *J Phys D Appl Phys* 40(9):2961–2971. <https://doi.org/10.1088/0022-3727/40/9/044>
35. Luo L, Girimaji SS (2002) Lattice Boltzmann model for binary mixtures [J]. *Phys Rev E* 66(3):035301-. <https://doi.org/10.1103/PhysRevE.66.035301>
36. Luo L, Girimaji SS (2003) Theory of the lattice Boltzmann method: Two-fluid model for binary mixtures [J]. *Phys Rev E* 67(3):036302-. <https://doi.org/10.1103/PhysRevE.67.036302>
37. McCracken ME, Abraham J (2005) Lattice Boltzmann methods for binary mixtures with different molecular weights [J]. *Phys Rev E* 71(4):046704-. <https://doi.org/10.1103/PhysRevE.71.046704>
38. Hussain MM, Li X, Dincer I (2008) A general electrolyte-electrode-assembly model for the performance characteristics of planar anode-supported solid oxide fuel cells [J]. *J Power Sources* 189(2):916–928. <https://doi.org/10.1016/j.jpowsour.2008.12.121>
39. Mastropasqua L, Donazzi A, Campanari S (2018) Development of a multiscale SOFC model and application to axially-graded electrode design [J]. *Fuel Cells* 19(2):125–140. <https://doi.org/10.1002/fuce.201800170>
40. Yahya A, Hammouda S, Slimene S et al (2022) Effect of cathode pulsating flow on mass transport and performance of solid oxide fuel cell [J]. *Int J Thermal Sciences* 174:107437. <https://doi.org/10.1016/j.ijthermalsci.2021.107437>
41. Huang J, Li ZY, Li N et al (2021) An approach combining the lattice Boltzmann method and Maxwell-Stefan equation for modeling multi-component diffusion [J]. *Phys Fluids* 33:1–17. <https://doi.org/10.1063/5.0059073>
42. Mahmood MA, Chaudhary TN, Farooq M et al (2023) Sensitivity analysis of performance and thermal impacts of a single hydrogen

- fueled solid oxide fuel cell to optimize the operational and design parameters [J]. *Sustain Energy Technol Assess* 57:1–10. <https://doi.org/10.1016/j.seta.2023.103241>
43. Zhao HF, Zhou J, Zong Z et al (2024) Three-dimensional reconstruction and optimization of porous fuel electrode in reversible solid oxide cells based on the Lattice Boltzmann method [J]. *Electrochim Acta* 476:1–14. <https://doi.org/10.1016/j.electacta.2023.143702>
44. Yahya A, Rabhi R, Dhahri H et al (2018). Numerical simulation of temperature distribution in a planar solid oxide fuel cell using lattice Boltzmann method [J]. *Power Technol* 338:402–415. <https://doi.org/10.1016/j.powtec.2018.07.060>
45. Xu H, Dang Z (2016) Lattice Boltzmann modeling of carbon deposition in porous anode of a solid oxide fuel cell with internal

reforming [J]. *Appl Energy* 178:294–307. <https://doi.org/10.1016/j.apenergy.2016.06.007>

Publisher's Note Springer Nature remains neutral with regard to jurisdictional claims in published maps and institutional affiliations.

Springer Nature or its licensor (e.g. a society or other partner) holds exclusive rights to this article under a publishing agreement with the author(s) or other rightsholder(s); author self-archiving of the accepted manuscript version of this article is solely governed by the terms of such publishing agreement and applicable law.